

Development of ZnO nanowire based CdTe thin film solar cells



Jonathan D. Major^{a,*}, Ramon Tena-Zaera^b, Eneko Azaceta^b, L. Bowen^c, K. Durose^a

^a Stephenson Institute for Renewable Energy, University of Liverpool, Liverpool L69 7ZF, UK

^b IK4-CIDETEC, Parque Científico y Tecnológico de Gipuzkoa, San Sebastián, Spain

^c G.J. Russell Microscopy Facility, Durham University, South Road, Durham DH1 3LE, UK

ARTICLE INFO

Keywords:

Nanowire
Photovoltaics
Cadmium Telluride
Solar

ABSTRACT

This work reports on the development of CdTe thin film solar cells grown on ZnO nanowire arrays. The focus was placed on utilising ZnO nanowire arrays as a replacement to the conventional ZnO thin film buffer layer, thereby requiring minimal alteration to the existing solar cell structure. Incorporation of nanowires was found to alter subsequent film growth and processing, with the nanowire dimensions changing device performance significantly. Shorter, ~100 nm, wires were found to produce particularly low device performance of < 0.5% whilst longer wires in the range 250–2000 nm were able to produce more functional cells. Working devices of up to 9.5% efficiency were achieved through the production of “embedded tip” nanowire solar cells. Variation of the nanowires length demonstrated that the nanowires were involved in carrier recombination and that this may be the performance limiting factor.

1. Introduction

Nanowires (NW) have attracted a great amount of interest for implementation in a range of electronic and opto-electronic devices [1,2]. By constraining carrier transport in two dimensions this allows carriers to be directed via the remaining unconstrained dimension. The NW arrays offer the potential for improved charge carrier mobility and reduced reflection, allowing improved optical collection [3]. For photovoltaics (PV) this has obvious benefits [1] but the implementation of nanowires in real solar cells is challenging. Whilst high efficiencies are often demonstrated for single nanowire devices [4,5], realisation of nanowire cells on a macroscopic scale is more difficult. Due to the high aspect ratio of nanowires, and the often challenging nature of their growth, their use adds an extra layer of complexity to already tricky solar cell fabrication processes. For CdTe solar cells the preferred implementation would be to grow CdTe nanowires and produce cells via the “core-shell” approach [6]. In this design the CdTe wires are coated with *n*-type CdS and transparent conductive oxide (TCO) layers to form a continuous *p*-*n* junction across the whole device, theoretically improving collection and reduce carrier recombination in the CdTe layer. There are a number of issues with this design however. Firstly it requires the CdTe solar cell to be grown in the inverted “substrate” geometry [7] (rather than more established “superstrate” geometry) which is lower efficiency and commonly results in back contacting issues [8]. Additionally growth of CdTe NWs is via the vapour-liquid-solid (VLS) mechanism which requires a catalyst layer such as gold [6],

or bismuth [9], may generate related impurity deep levels [10] and thus increase recombination within the CdTe. There is also often the need for a CdTe thin film under-layer to be used for growth [6], in which case some of the NW enhancement may be compromised due to recombination in the thin film layer.

An alternative approach is to use a material which is more easily deposited as a NW than CdTe as the basis for NW incorporation. Whilst some authors have attempted this by using CdS nanopillars coupled to a CdTe thin film [11], this too requires the VLS growth route and thus the inclusion of Au seed layers. In contrast ZnO nanowires may be grown easily via low-temperature, self-assembly electrochemical deposition, without the requirement for contaminating seed layers [12]. The incorporation of ZnO nanocones as a replacement for the CdS layer has previously been reported [13], but these devices demonstrated very low conversion efficiency of < 3.2% as may be expected due to the inherently poor quality of the ZnO/CdTe junction [14]. Here we take a different approach by simply maintaining ZnO in its usual implementation. ZnO films are commonly included in a number of thin film PV technologies such as CdTe or CuIn_xGa_{1-x}Se₂ (CIGS) as what is typically referred to as a resistive “buffer” layer [15], located between the *n*-type window layer and the TCO front contact. This layer serves to improve device performance as it allows the window layer, typically CdS, to be reduced in thickness without any loss of device performance. Optimising the thickness of the resistive buffer layer requires a trade-off between the benefits yielded by the layer and the additional series resistance it produces. For example a relatively thick buffer layer >

* Corresponding author.

E-mail address: jon.major@liverpool.ac.uk (J.D. Major).

<http://dx.doi.org/10.1016/j.solmat.2016.10.024>

Received 26 July 2016; Received in revised form 7 October 2016; Accepted 9 October 2016

Available online 24 October 2016

0927-0248/© 2016 The Authors. Published by Elsevier B.V. This is an open access article under the CC BY license (<http://creativecommons.org/licenses/by/4.0/>).

500 nm may block shunting pathways and improve band alignments, but the overall performance could decrease due to resistive losses. The use of nanowires as the buffer layer should allow nanowire lengths greater than the equivalent film thickness to be utilised. This serves to the same purpose as the planar buffer layer, but without hindering current transport across the junction. It may also generate a physical separation between the CdTe layer and front contact, making front to back contacting shorting extremely difficult. This is in addition to the inherent light trapping properties of the nanowires which should allow this nanowire buffer layer to play a dual role.

This paper reports on the development of CdTe solar cells of up to 9.5% efficiency incorporating ZnO NWs deposited by a low temperature electrochemical deposition route. The respective challenges for production as well as electrical and optical properties of NW and planar equivalent cells will be discussed.

2. Materials and methods

2.1. ZnO nanowire deposition

ZnO NW arrays of varying dimensions were electrodeposited on FTO-coated glass substrates which had a 100 nm ZnO film deposited on the surface by RF sputtering. NWs were produced by the reduction of dissolved molecular oxygen in zinc chloride aqueous solutions [16]. In particular, 5×10^{-4} M ZnCl_2 (> 98.0%), 0.1 or 2 M KCl (> 99.5%) ultrapure aqueous solutions, saturated with bubbled oxygen, were used. The KCl concentration was varied (i.e. 0.1 and 2 M) in order to tailor the nanowire growth mechanism [15]. The nanowire length was varied by modifying the charge density applied during the electro-deposition.

2.2. Solar cell fabrication

CdS layers were deposited at 200 °C by RF sputtering at a power of 60 W and with a thickness of ~200 nm. ~4 µm thick CdTe layers were then deposited via close space sublimation (CSS) under 25 Torr of nitrogen using source and substrate temperatures of 605 °C and 510 °C respectively. A 30 s nitric-phosphoric (NP) acid etch was carried out prior to post-growth chloride activation treatment to enhance the Cl inter-diffusion [17]. The CdCl_2 (or for later samples MgCl_2 [18]) activation step was performed in air in the range 410–450 °C and 20–40 min, the time and temperature being optimised for different sample structures. Following this the samples were etched in NP solution for a further 15 s prior to application of a matrix of gold back contacts deposited by thermal evaporation.

2.3. Thin film and device characterisation

The cross sections of the ZnO nanowire arrays and solar cells were analysed using an ULTRA plus ZEISS field emission scanning electron microscope (FESEM). For focussed ion beam (FIB) milling a FEI Helios Nano Lab 600 Dual Beam system, equipped with a focused 30 kW Ga liquid metal ion source was used. Samples were then transferred to a Hitachi SU70 SEM from imaging and electron beam induced current (EBIC) analysis via a Matelect ISM5 specimen current amplifier set to a 10 nA measurement range. Beam conditions used for EBIC analysis were 5 kV with a beam current of 0.9 nA. Optical reflectance measurements were performed using a Shimadzu Solidspec 3700 spectrophotometer with an integrating sphere. Complete cell characterisation was carried out using a Bentham PVE300 system for external quantum efficiency (EQE) measurements, an AM1.5 calibrated TS space systems solar simulator for current voltage (*JV*) analysis and a Solatron SI1260 impedance analyser for capacitance voltage (*CV*) measurements.

3. Results

3.1. Initial test samples

For initial device testing samples were produced utilising a range of nanowire dimensions and growth conditions to assess the most suitable configuration. CdTe and CdS deposition parameters were kept identical to that for deposition on typical ZnO films, however it was anticipated this was likely to be non-optimal for the ZnO NW solar cells due to variations in film growth rates on the different surfaces. Three NW array types were initially compared as shown in Fig. 1a: i) “short” ~100 nm NWs, ii) “long type I” ~1 µm NWs with growth condition I and iii) “long type II” ~1 µm NWs with growth condition II. The difference between the I and II NW array type is the growth conditions. For II NW array type, growth along the radial direction (i.e. lateral growth [19]), which thickens the NWs, was intentionally promoted. In contrast, for I NW array type growth occurs primarily along the longitudinal direction of the NW. For comparison a 100 nm thick ZnO film buffer layer with no NW coating was used for a control device. Complete solar cell structures were deposited as described in the experimental section using each of the substrate types. These initial test devices were CdCl_2 treated using standard cell processing conditions (25 min at 410 °C) for typical planar devices with ZnO thin films. Gold back contacts used for the purpose of these initial test cells were small dot contacts of 2 mm diameter. EQE and *JV* analysis of each device was then carried out with curves for the highest efficiency contacts shown in Fig. 1b and c respectively. It is important to note that for test contacts of this size determined J_{sc} values from *JV* curves are often over-estimated due to the problem of edge collection effects from the dot contacts. Because the back surface has been NP etched and is thus slightly tellurium-rich, the area of the contact is effectively extended and thus the J_{sc} is typically overestimated however V_{OC} and *FF* are unaffected. This is a common problem when small area contacts are used. Hence for this initial set of test devices we are only using a comparative analysis rather than quoting absolute J_{sc} or efficiency values.

Initial device testing showed that cell performance was dramatically reduced by the incorporation of NW arrays. The peak efficiency decreased from > 11% with a V_{OC} of 0.80 V for the planar cells to < 2.4% for all NW cells with a peak V_{OC} of 0.46 V, and other performance parameters, *FF* and J_{sc} , similarly degraded. While none of the NW samples performed well the 1 µm type II NW array based device (< 2.4%, 0.46 V) was significantly better than the 100 nm NW (< 1.2%, 0.38 V) and particularly that based on 1 µm type I NW array (< 0.5%, 0.22 V). *JV* curves (Fig. 1c) imply an overall reduction in the quality of the junction for NW devices, while EQE curves (Fig. 1b) give some indication of the cause. The overall EQE response is reduced for the nanowire samples, corroborating the lower J_{sc} values. It is notable however that for the ZnO film device there is a distinct drop in EQE below the CdS band edge (~520 nm). For the ZnO nanowire based devices there is little discrepancy in performance above or below the CdS band edge, indicating that for the NW cells the CdS thickness is almost negligible. There are three possible explanations for this outcome either; i) the CdS growth rate is significantly reduced on NW arrays resulting in a decreased as-grown film thickness, ii) CdS/CdTe inter-diffusion is greatly increased due to the increased surface roughness or iii) re-evaporation of CdS occurs during CdTe deposition due to the increased surface area of the films. As CdS was clearly visible following sputtering deposition on the NWs and optical transmission measurements confirmed its presence, the CdS layer must be primarily lost during CdTe deposition. Enhanced CdS/CdTe inter-diffusion rather than re-evaporation from the surface seems the most probable mechanism given the sublimation temperature of CdS exceeds that of CdTe. This loss of CdS is likely to have significantly contributed to the reduced device performance as ZnO/CdTe junctions are of much lower

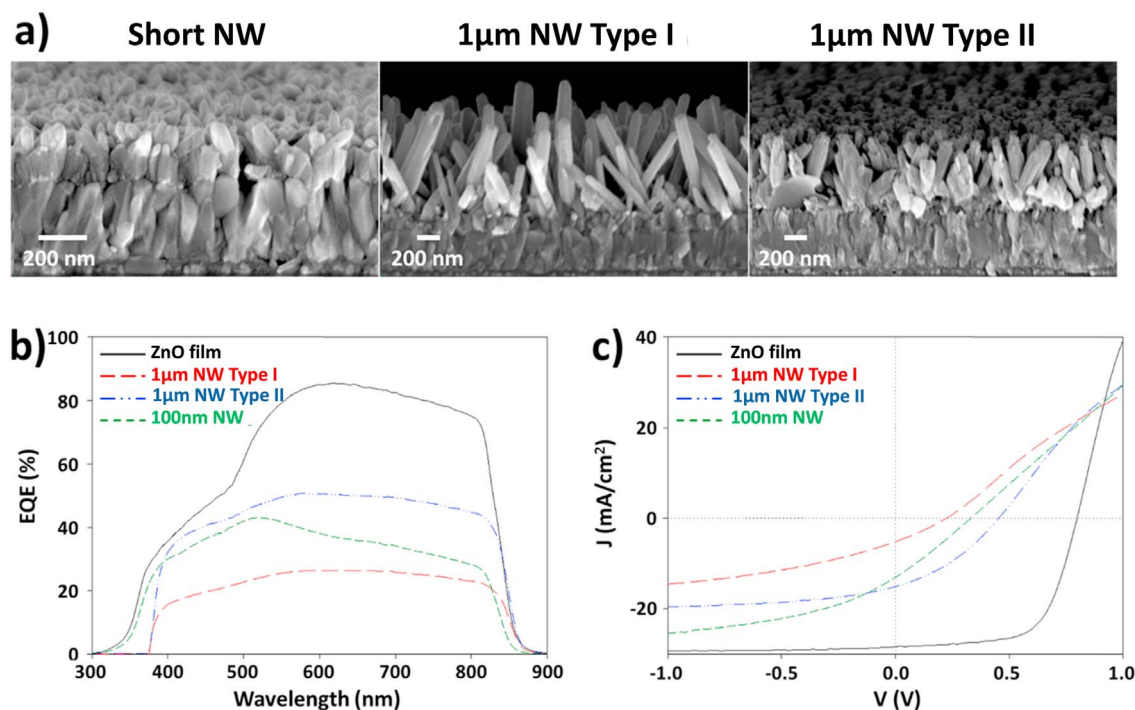


Fig. 1. Comparison of the three ZnO nanowire types, 100 nm long, 1 µm long type I and 1 µm long type II with an additional lateral overgrowth. a) SEM images, b) EQE analysis and c) *JV* curves for highest efficiency contacts from cells produced using each of different nanowire substrate types as well as a ZnO film comparison.

quality than CdS/CdTe junctions [14]. This is the root cause of the low performance in the NW cells but is indicative of a fabrication issue rather than a fundamental limitation of the NWs themselves.

Additional characterisation of these solar cell structures was then carried out to determine the structural and optical properties in more detail. Fig. 2a,b show SEM images of a FIB milled cell cross section for a sample deposited on the 1 µm type I (no lateral growth) nanowires. The CdTe layer has deposited on the tips of the nanowires with only a small amount of penetration down the nanowire shaft. The junction can clearly be seen to form with the nanowires at the region surrounding the tips. Clear physical separation between the CdTe layer and TCO layers exists, demonstrating all extracted carriers must flow through the nanowires. No evidence of a CdS layer can be seen, in good agreement with the EQE analysis for this sample and again indicative that the primary loss mechanism has been through CdS consumption or re-sublimation.

X-ray diffraction (XRD) analysis of CdTe layers, Fig. 2c, showed a distinct change in the orientation of the films for deposition on ZnO NWs compared to deposition onto a ZnO thin film. CdTe layers deposition onto ZnO films gave films with a stronger $\langle 111 \rangle$ orientation. Deposition onto NWs gave a film with much stronger $\langle 220 \rangle$, $\langle 331 \rangle$ and $\langle 422 \rangle$ reflections, with an associated reduction in the standard deviation of the texture coefficients. This demonstrated that as well as impacting upon the CdS layer, the presence of the NWs had a clear impact on CdTe film formation.

To assess the anti-reflection potential of the NW substrates the front surface reflection properties were compared via measurement of optical reflectance as shown in Fig. 2d. The two samples with long 1 µm NWs show a strong reduction in reflectance compared to the planar film and short 100 nm NW samples. For the type II 1 µm NWs the reflectance is $< 1.9\%$ across the useable wavelength range of a CdTe solar cell. This reduced reflection is a well-established effect due to optical quenching associated with the textured surface and is therefore determined by the nanowire dimensions. This data does show the capability of the NWs to minimise the reflection loss and, in theory, should result in the improved optical collection of these cells.

3.2. Device development

After the initial sample set a few points were noted. Firstly, whilst the device performance was greatly decreased by the incorporation of ZnO NWs, working devices were attainable and that due to the physical separation of the CdTe and TCO layers this was a clear demonstration that electron transport was occurring via NWs. Secondly a large amount of the performance loss may have been due to variations in processing conditions, *i.e.* stability of the CdS layer, optimal CdCl₂ treatment temperature and time. It seemed highly probable this was caused by the significant change in surface roughness which occurred due to the incorporation of NWs. As well as influencing the growth of CdS and CdTe layers there is also the potential for the NW incorporation to alter the way these layers intermix, both during CdTe deposition and chloride treatment, which is a key factor in junction formation. An extensive period of device optimisation was then undertaken with a number of distinct processing changes, compared to typical planar device fabrication, being made. Initially the CdS deposition time was doubled to ensure a CdS layer was present even if growth rates were decreased or CdS/CdTe inter-diffusion increased. Devices with increased CdS thickness were found to show an improved *JV* curve shape (*i.e.* higher FF) but were still low performance $< 1\%$ and appeared “under-treated” (*i.e.* had not had sufficient CdCl₂ treatment). As a result, the CdCl₂ annealing temperature was increased from the typical 410–450 °C which was found to yield improved device performance for NW based devices. Whilst this may seem a small temperature variation, in the context of chloride treatment this is actually a significant increase. Planar samples treated at 450 °C are over-treated and even show signs of film delamination. This emphasised though that the incorporation of NWs had significantly shifted the processing conditions.

Following these process modifications, a second set of solar cells were produced by using varied NW arrays which were electrodeposited with no additional lateral growth conditions (*i.e.* they were similar to the type I NWs). These NW arrays were designated as either type A or type B with either long (*i.e.* 1 µm, AI and BI) or short (*i.e.* 100–150 nm,

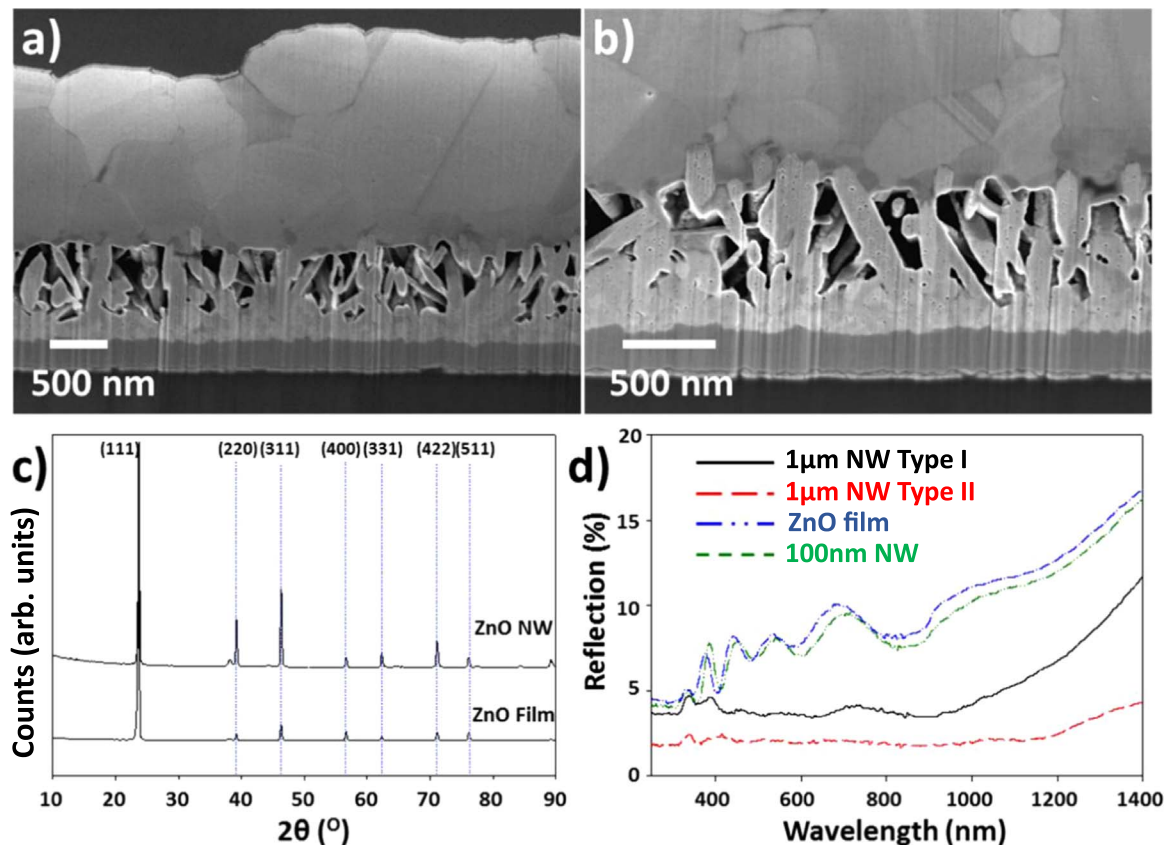


Fig. 2. Structural and optical characterisation showing a), b) cross sectional SEM micrographs of FIB milled device cross sections, c) X-ray diffraction spectra for CdTe layers deposited on a ZnO film and onto ZnO nanowire substrate and d) Optical reflectance curves of nanowire and planar ZnO film on TCO substrates.

AII and BII) variants. Type A nanowire arrays had a higher degree of length variation and greater spacing between NWs than for the type B. SEM micrographs of these NW types are shown in Fig. 3. For each NW type, the post-growth CdCl₂ treatment time was optimised in the range 20–40 min at 450 °C so as to compensate for any process variations arising from the different morphologies of the ZnO NWs. For these devices grids of larger 0.25 cm² gold back contacts were used to improve the accuracy of J_{sc} values. Associated peak device performance parameters are given in Table 1 with average performance parameters for the same devices given in Table 2. JV and EQE curves are given in Fig. 4a and b. Capacitance voltage (CV) measurements were used to calculate carrier concentration, N_a , vs depletion width, W_d , [20] which is given in Fig. 4c and with a normalised version in 4d. Doping density values extracted directly from the gradient Mott-Schottky $1/C^2$ vs V plots are also given in Table 1.

Significant differences in cell performance were observed for different NW array types. From EQE measurements (Fig. 4b) arrays of short NWs (AII and BII) gave a characteristic buried homo-junction response (i.e. EQE peak occurring at long λ) [21,22], indicating that the photovoltaic junction was formed deep in the CdTe layer away from the CdS/CdTe interface. This accounts for the poor device performances observed and in particular the low J_{sc} values obtained. In contrast, arrays of long NWs (AI and BI) led to devices which display the desired hetero-junction response as indicated by the EQE measurement. As a result, the device performance was significantly improved giving efficiency values of up to 6.36% for the BI NW arrays and 4.32% for the AI NW arrays. Unlike for previous devices the CdS cut-off at ~ 525 nm is clearly visible. Indeed, for these samples the cut-off is more severe than ideal, indicating CdS thickness could likely be reduced to minimise optical losses and improve device J_{sc} values. Un-normalised depth doping profiles from CV analysis, Fig. 4c, show good agreement to the EQE data. These imply that the rapid increase in doping associated with the junction [23] occurs away from the front surface

at a depth of approximately 1 μm and 2 μm for the devices based on short NW arrays (i.e. BII and AII, respectively). The shape of the JV curves further highlights the difference in performance between the long and short NW types. The longer NWs (i.e. AI and BI) have a high degree of rollover in the forward bias region indicating a poor, non-ohmic, back contact [24]. This may be partially responsible for the low V_{oc} values obtained, < 0.70 V, in comparison to that expected for comparable planar devices, ~ 0.80 V. The doping profiles display a drop in doping at the back surface region in all samples. This drop in doping at may be the cause of the poor back contacting, but this occurs only in NW based devices is currently unclear.

The device based on AI type NW array shows a decrease in the FF and V_{oc} in comparison that based on BI type one. This is primarily attributable to the low doping density (Table 1) of the former device, $2.22 \times 10^{13} \text{ cm}^{-3}$, compared to the latter device, $2.91 \times 10^{14} \text{ cm}^{-3}$. This may be related to a lower carrier density for the ZnO nanowires in type A arrays due to electrodeposition from a lower concentration KCl solution (i.e. 0.1 M) [25] being used to produce and greater spacing between NWs. In comparison the devices with shorter NWs (i.e., types AII and BII) have higher doping density than those with long NWs (i.e.; type AI and BI), $5.28 \times 10^{13} \text{ cm}^{-3}$ and $6.53 \times 10^{13} \text{ cm}^{-3}$ respectively, but their cell performance is critically compromised by the formation of the buried junction. The JV curves for these cells have a good shape, and hence high FF , but J_{sc} is extremely low at $< 2 \text{ mA/cm}^2$. The most likely interpretation for the cause is again though modification of the CdS/CdTe inter-diffusion and thus the effectiveness with which an $n\text{-CdS}/p\text{-CdTe}$, rather than a $n\text{-CdTe}/p\text{-CdTe}$, junction forms. Untreated CdTe cells are often seen to display buried homo-junction behaviour, which is converted to hetero-junction behaviour following chloride treatment [21]. If the CdS inter-diffusion is drastically modified by the presence of the NW under layer, this conversion may simply not occur. The presence of significant rollover for devices based on long NWs (i.e. AI and BI), but not on short (i.e. AII and BII) is rather puzzling as this

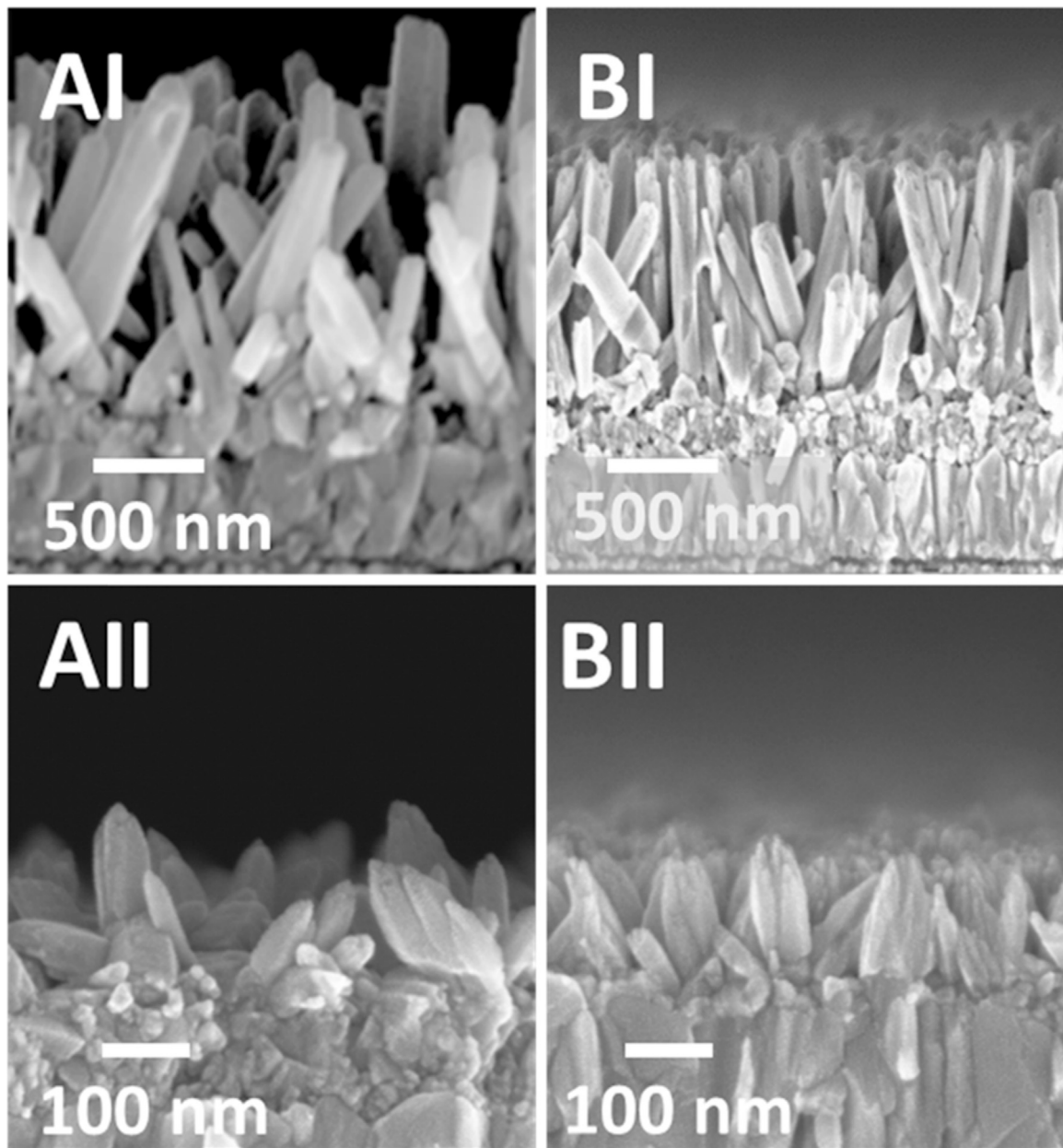


Fig. 3. SEM micrographs of the long (AI and BI) and short (AII and BII) ZnO nanowire types used for cell deposition. Type A nanowire arrays have a higher degree of length variation and greater spacing between NWs than for the type B.

Table 1
Solar cell performance parameters extracted from JV curves for highest efficiency contacts shown in Fig. 3.

Nanowire type	Peak efficiency (%)	Fill factor (%)	J _{SC} (mA/cm ²)	V _{OC} (V)	N _a (cm ⁻³)
Type AI (1 μm)	4.32	47.01	16.20	0.60	2.22 × 10 ¹³
Type BI (1 μm)	6.36	59.07	18.20	0.68	2.91 × 10 ¹⁴
Type AII (100 nm)	0.62	58.08	2.61	0.44	6.53 × 10 ¹³
Type BII (100 nm)	1.46	52.09	7.23	0.44	5.29 × 10 ¹³

is predominately a back contact barrier effect and in all cases back contact preparation was identical. Roussillon et al. [26] posited an

Table 2
Average performance parameters extracted from JV curves for all device contacts (N=9).

Nanowire type	Average efficiency (%)	Fill factor (%)	J _{SC} (mA/cm ²)	V _{OC} (V)
Type AI (1 μm)	1.6 +/-1.2	30.2 +/-6.8	10.8 +/-3.4	0.42 +/-0.11
Type BI (1 μm)	4.6 +/-1.6	49.9+/-6.8	14.4 +/-3.6	0.62 +/-0.03
Type AII (100 nm)	0.2 +/-0.2	46.1 +/-11.3	1.2 +/-0.7	0.4 +/-0.1
Type BII (100 nm)	0.3 +/-0.3	47.9 +/-3.4	1.8 +/-1.8	0.4 +/-0.02

effect termed as “reach through band bending” wherein the buffer layer and back contacting are linked, but we are unaware of instances where a change in a cell buffer layer has resulted in the generation of rollover. Fig. 5a–c show cross sectional SEM images of completed solar cell

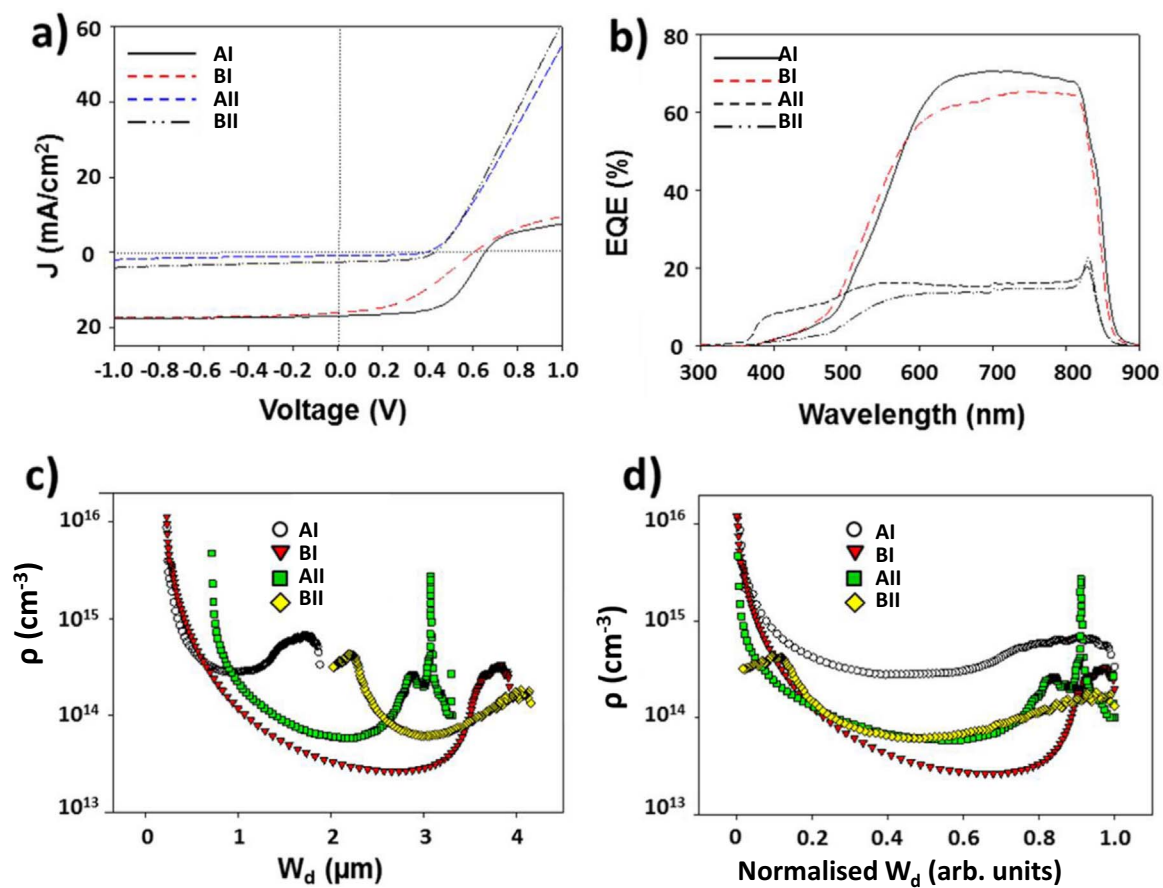


Fig. 4. Electrical characterisation for cells based on type A and type B NWs a)EQE and b) JV curves for highest efficiency contacts from each of different nanowire substrate types. Hole density (ρ) vs. c) depletion width (W_d) and d) normalised depletion width determined from C-V measurements.

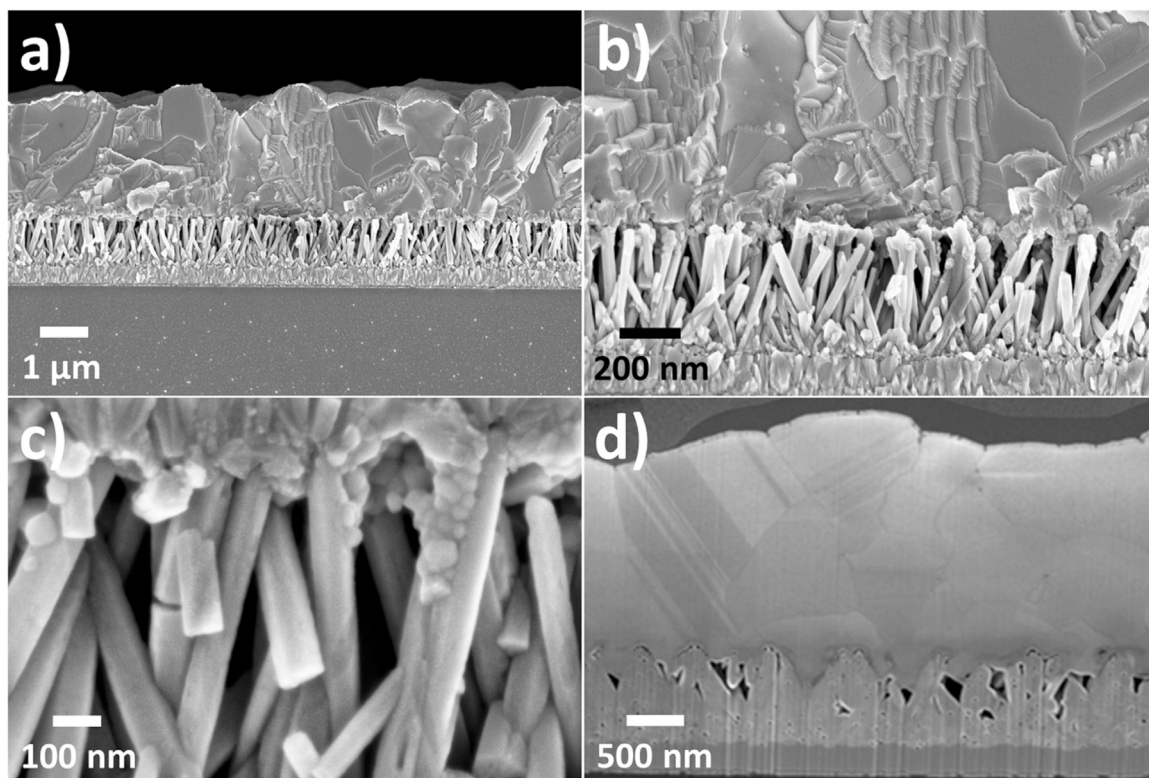


Fig. 5. SEM cross section images of completed 'embedded tip' devices comprising CdTe and CdS layers sitting on top of arrays of type A ZnO NWs. a) – c) show cleaved cross sections at increasing magnification and d) shows a focused ion beam cross section showing the NW tip penetration into the CdS/CdTe layers.

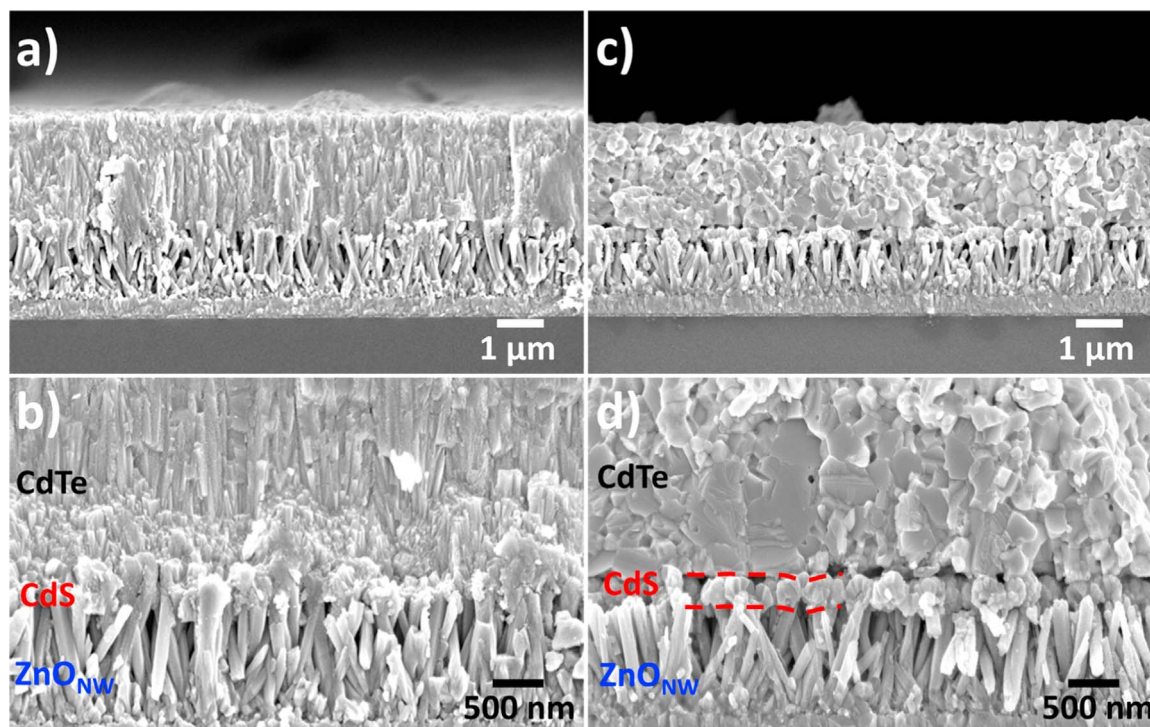


Fig. 6. SEM cross section micrographs of devices comprising CdTe and CdS layers deposited by low temperature CSS deposition on top of arrays of type A ZnO NWs. a) and b) show as-deposited samples prior to CdCl₂ treatment c) and d) samples following CdCl₂ processing

structures on type B nanowires, while Fig. 5d shows a focus ion beam (FIB) milled cross section of the same device. It can clearly be seen from these images that the CdTe layer has again not produced a conformal coating of the NWs but rather has formed a thin film giving an “embedded tip” solar cell structure. Penetration of the NWs into the interface can clearly be seen but in addition the CdS layer is now visible and has only coated the ends of the NWs rather than their whole length. In order to gain a further insight into the reasons behind of the lack of penetration of the CdTe into the ZnO nanowire array structure, the cross section of samples with CdTe deposited by different techniques and conditions were analysed.

Solar cells fabricated using low temperature, $T_{\text{Source}}=450\text{ }^{\circ}\text{C}$, CSS deposition were assessed via cross-sectional SEM analysis to see if the smaller CdTe grain size resulted in penetration into the NW array. Both as deposited (Fig. 6a and b) and following CdCl₂ treatment (Fig. 6c and d) were compared. The as-deposited CdTe layers had a very small columnar grains as is typical for low-temperature deposition [27] but even at this grain size there is little penetration into the NW array was observed. Following CdCl₂ treatment significant recrystallization and grain growth occurs as expected [28] but a discontinuity was seen to form between the CdS and CdTe layers. Indeed solar cells deposited at lower CSS temperatures were found to always display particularly low performance, < 0.1%, due to this inability to form a consistent physical junction. Similar results were also found when sputtered CdTe layers were used, with little penetration into the NW array being observed. Therefore, it was found that when the NW density is sufficiently high, CdS and CdTe deposition essentially proceeds as if occurring on a planar ZnO film, regardless of deposition technique (i.e. RF sputtering, CSS) or growth conditions utilised.

3.3. ZnO NW length variation

Following the results of the 2nd sample set, the type B nanowires had been identified as the most suitable for incorporation into CdTe solar cells. A final set of samples was then produced where the length of the NWs was varied in an attempt to determine the impact of NW

Table 3

Solar cell performance parameters extracted from JV curves for highest efficiency contacts shown in Fig. 7.

Nanowire length	Peak efficiency (%)	Fill factor (%)	J_{sc} (mA/cm ²)	V_{oc} (V)
0 nm (ZnO film)	9.99	63.93	19.78	0.79
~250 nm	9.53	65.25	19.76	0.76
~500 nm	8.01	65.09	19.64	0.69
~1 μm	7.48	60.86	18.93	0.66
~2 μm	5.40	49.78	18.39	0.59

length on device performance. Four different ZnO NW samples were used to produce solar cells with the NW length varying from ~250–2000 nm, a ZnO film was also used for comparison. Solar cell deposition conditions used were the same as for the previous sample set but following the in-house development of an MgCl₂ alternative to CdCl₂ [18], MgCl₂ treatment was instead used (there being no difference in the device performance levels following MgCl₂ or CdCl₂ treatment) with the treatment time and temperature being optimised for each NW substrate type. As previously, solar cells which incorporated NWs were found to require a higher temperature anneal (450 °C) than planar equivalents (410 °C) to achieve optimal performance. Peak performance parameters from the five substrate types compared are given in Table 3 with associated JV and EQE data given in Fig. 7a and b.

For the shortest NW length used, 250 nm, efficiency of up to 9.53% was achieved. This represents, to the authors knowledge, the highest such efficiency reported for CdTe solar cells which incorporate NWs. However, tellingly this efficiency is below that for the equivalent planar solar cell 9.99%. From the performance parameters it can be seen that increasing the NW length corresponds to a decrease in performance, primarily through a reduction in the V_{oc} from 0.79 to 0.59 V with increasing NW length, although the sample with ~2 μm NWs does also show a significantly reduced fill factor. In contrast the J_{sc} is largely maintained even for ~2 μm NWs, 18.39 mA/cm², compared to a planar

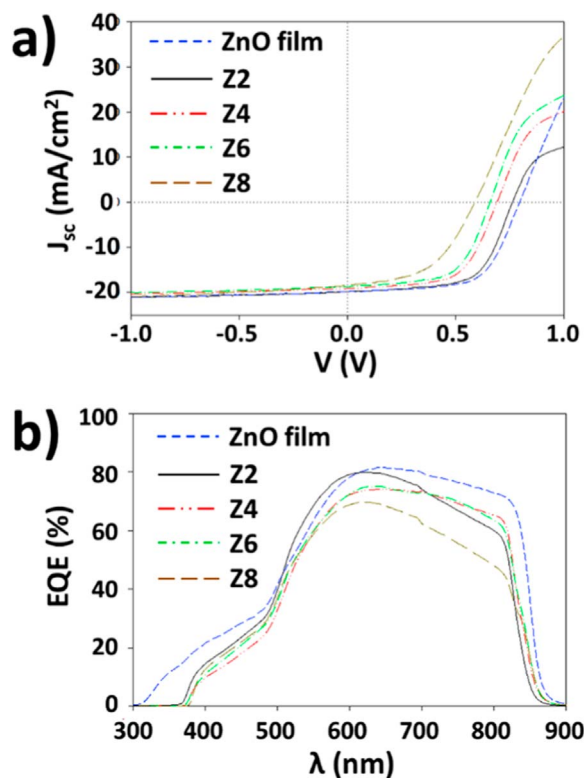


Fig. 7. a) JV and b) EQE curves for highest efficiency contacts from cells with systematically varied NW lengths 250–2000 nm with a comparative ZnO thin film device.

ZnO film solar cell, 19.78 mA/cm². Electron beam induced current (EBIC) analysis of solar cell cross sections allows the p-n junction position to be analysed [29]. Fig. 8 shows secondary electron (a and c)

and combined EBIC/secondary electron images (b and d) of cross sections for solar cells with 250 nm and 500 nm NWs. The green regions in figures b and d represent the areas of high current and thus the location of the PV junction. Quantified EBIC data was not able to be extracted but the generated EBIC signals were measured utilising the same amplifier current range (10 nA), implying a similar level of collection efficiency for both samples. Both solar cells showed the PV junction was formed at the CdS/CdTe interface region, with there being negligible change in the qualitative EBIC signal. Additionally no collection occurred from the NWs confirming they were merely acting as current conduits and explains why there was little change in the J_{sc} . The predominantly V_{oc} based loss mechanism seen for NW solar cells also appeared not to be a purely resistive effect, as R_s determined for the ZnO planar solar cell (3.8 Ω) is higher or equivalent to that determined for the NW based solar cells (3.1–3.8 Ω). From the JV curves (Fig. 7a) there is again the presence of increased rollover for NW solar cells, whereas the planar solar cells display little in the way of rollover. Whilst this rollover may be anticipated to impact V_{oc} , the degree of the V_{oc} loss is too severe to be accounted for by this level of rollover. Instead we believe the losses observed for the NW based solar cells are an indication of some form of recombination loss occurring within the ZnO NWs. We may ascribe the losses seen between the ZnO film and the 250 nm NW sample to increases in interfacial recombination, but the variation between samples with 250 nm to 2 μ m, where the interfacial recombination should be constant, must be due to recombination in the wires. As the length of the wire is increased, so too does the carrier path length through the wire and resultant recombination is increased, reducing the V_{oc} . This demonstrates that in theory whilst NWs should transfer current with minimal losses, practically there may be limitations to their behaviour. Indeed, significant variations in the local conductivity were previously mapped in the cross section of the ZnO electrodeposited nanowires by infrared nanoscopy [30] and such variations may be problematic.

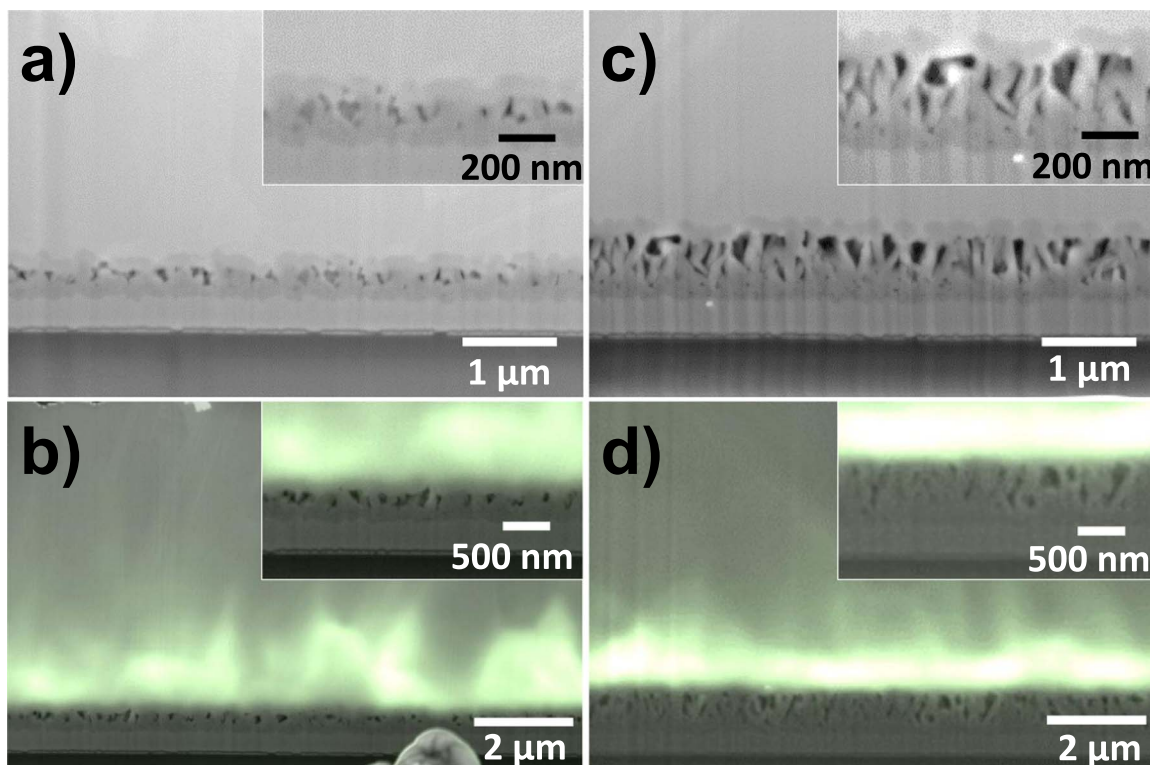


Fig. 8. SEM micrographs and EBIC images of samples cells with ~250 nm a-b) and ~500 nm NWs c-d). Insets show a higher magnification of the junction region. EBIC current signal data (green) is overlaid on secondary electron images to show junction position. Areas of highest contrast represent most efficient collection regions. (For interpretation of the references to color in this figure legend, the reader is referred to the web version of this article.)

4. Conclusion

This work demonstrates a route to achieving close to 10% efficiency for CdTe thin film solar cells which incorporate ZnO NWs. The NW embedded tip structure shows promise with efficiency of up to 9.53% being achieved. Whilst this resulted in a very significant improvement versus previous reports [30], performance is still below that from the comparable planar film equivalent due to problems associated with interfacial recombination and additional recombination in NWs. In order to improve the performance further and surpass the ZnO thin film equivalent work is required to understand to exactly what extent the nanowire related recombination limits the performance, can such recombination be overcome or will it always prove a limiting factor. It may be that doping the NWs is in some way required to improve conductivity or alternatively that pre-treatment of the CdS/NW interface is required to minimise recombination centres that arise there. The potential benefits of NW incorporation such as improved optical performance, thereby allowing absorber thickness reduction, make this more than worthy of further investigation though.

Acknowledgements

This work was funded by the UK Engineering and Physical Sciences Research Council Grant number EP/J017361/1. The data which supports the findings of this work is available through the University of Liverpool RDM DataStore or from the author by request.

References

- [1] Z. Fan, J.C. Ho, B. Huang, One-Dimensional Nanostructures for Energy Harvesting, in: One-Dimensional Nanostructures, John Wiley & Sons, Inc., 2012, pp. 237–270.
- [2] Y. Li, F. Qian, J. Xiang, C.M. Lieber, Nanowire electronic and optoelectronic devices, *Mater. Today* 9 (2006) 18–27.
- [3] L. Cao, J.S. White, J.-S. Park, J.A. Schuller, B.M. Clemens, M.L. Brongersma, Engineering light absorption in semiconductor nanowire devices, *Nat. Mater.* 8 (2009) 643–647.
- [4] T.J. Kempa, B. Tian, D.R. Kim, J. Hu, X. Zheng, C.M. Lieber, Single and Tandem Axial p-n Nanowire Photovoltaic Devices, *Nano Lett.* 8 (2008) 3456–3460.
- [5] B. Tian, T.J. Kempa, C.M. Lieber, Single nanowire photovoltaics, *Chem. Soc. Rev.* 38 (2009) 16–24.
- [6] B.L. Williams, A.A. Taylor, B.G. Mendis, L. Phillips, L. Bowen, J.D. Major, K. Durose, Core-shell ITO/ZnO/CdS/CdTe nanowire solar cells, *Appl. Phys. Lett.* 104 (2014) 053907.
- [7] L. Kranz, C. Gretnener, J. Perrenoud, R. Schmitt, F. Pianezzi, F. La Mattina, P. Bloesch, E. Cheah, A. Chirila, C.M. Fella, H. Hagendorfer, T. Jaeger, S. Nishiwaki, A.R. Uhl, S. Buecheler, A.N. Tiwari, Doping of polycrystalline CdTe for high-efficiency solar cells on flexible metal foil, *Nat. Commun.* 4 (2013) 2306.
- [8] B.L. Williams, J.D. Major, L. Bowen, L. Phillips, G. Zoppi, I. Forbes, K. Durose, Challenges and prospects for developing CdS/CdTe substrate solar cells on Mo foils, *Sol. Energy Mater. Sol. Cells* 124 (2014) 31–38.
- [9] S.K.C. Lee, Y. Yu, O. Perez, S. Puscas, T.H. Kosel, M. Kuno, Bismuth-assisted CdSe and CdTe nanowire growth on plastics, *Chem. Mater.* 22 (2010) 77–84.
- [10] S.H. Wei, S.B. Zhang, Theoretical Study of Doping Limits of CdTe: Preprint, in: Proceedings of the 2001 NCPV Program Review Meeting, Lakewood, 2001, pp. 1–4.
- [11] Z. Fan, H. Razavi, J.-w. Do, A. Moriwaki, O. Ergen, Y.-L. Chueh, P.W. Leu, J.C. Ho, T. Takahashi, L.A. Reichertz, S. Neale, K. Yu, M. Wu, J.W. Ager, A. Javey, Three-dimensional nanopillar-array photovoltaics on low-cost and flexible substrates, *Nat. Mater.* 8 (2009) 648–653.
- [12] R. Tena-Zaera, J. Elias, C. Levy-Clement, ZnO nanowire arrays: optical scattering and sensitization to solar light, *Appl. Phys. Lett.* 93 (2008) 233119.
- [13] S.H. Lee, X.G. Zhang, C.M. Parish, H.N. Lee, D.B. Smith, Y. He, J. Xu, Nanocone tip-film solar cells with efficient charge transport, *Adv. Mater.* 23 (2011) 4381–4385.
- [14] G.T. Koishiyev, J.R. Sites, Effect of weak diodes on the performance of CdTe thin-film modules, in: Proceedings of the 34th IEEE Photovoltaic Specialists Conference, 2009, pp. 1978–1981.
- [15] C.S. Ferekides, R. Mamazza, U. Balasubramanian, D.L. Morel, Transparent conductors and buffer layers for CdTe solar cells, *Thin Solid Films* 480 (2005) 224–229.
- [16] R. Tena-Zaera, J. Elias, C. Levy-Clement, I. Mora-Sero, Y. Luo, J. Bisquert, Electrodeposition and impedance spectroscopy characterization of ZnO nanowire arrays, *Phys. Status Solidi A – Appl. Mat.* 205 (2008) 2345–2350.
- [17] J.D. Major, Y.Y. Proskuryakov, K. Durose, Impact of CdTe surface composition on doping and device performance in close Space sublimation deposited CdTe solar cells, *Prog. Photovolt.* 21 (2013) 436–443.
- [18] J.D. Major, R.E. Treharne, L.J. Phillips, K. Durose, A low-cost non-toxic post-growth activation step for CdTe solar cells, *Nature* 511 (2014) 334–337.
- [19] J. Elias, R. Tena-Zaera, C. Levy-Clement, Electrochemical deposition of ZnO nanowire arrays with tailored dimensions, *J. Electroanal. Chem.* 621 (2008) 171–177.
- [20] P. Blood, J. Orton, The Electrical Characterisation of Semiconductors: Majority Carriers and Electron States, Academic Press, London, 1992.
- [21] J.D. Major, L. Bowen, R. Treharne, K. Durose, Assessment of photovoltaic junction position using combined focused ion beam and electron beam-induced current analysis of close space sublimation deposited CdTe solar cells, *Prog. Photovolt.* 22 (2014) 1096–1104.
- [22] J.D. Major, K. Durose, Study of buried junction and uniformity effects in CdTe/CdS solar cells using a combined OBIC and EQE apparatus, *Thin Solid Films* 517 (2009) 2419–2422.
- [23] J.V. Li, A.F. Halverson, O.V. Sulima, S. Bansal, J.M. Burst, T.M. Barnes, T.A. Gessert, D.H. Levi, Theoretical analysis of effects of deep level, back contact, and absorber thickness on capacitance-voltage profiling of CdTe thin-film solar cells, *Sol. Energy Mater. Sol. Cells* 100 (2012) 126–131.
- [24] A.R. Davies, J.R. Sites, Ieee, Effects of non-uniformity on rollover phenomena in CdS/CdTe solar cells, in: Proceedings of the 33rd IEEE Photovoltaic Specialists Conference, 2008, pp. 242–244.
- [25] R. Tena-Zaera, J. Elias, C. Levy-Clement, C. Bekeny, T. Voss, I. Mora-Sero, J. Bisquert, Influence of the Potassium Chloride Concentration on the Physical Properties of Electrodeposited ZnO Nanowire Arrays, *J. Phys. Chem. C* 112 (2008) 16318–16323.
- [26] Y. Roussillon, D.M. Giolando, V.G. Karpov, D. Shvydka, A.D. Compaan, Reach-through band bending in semiconductor thin films, *Appl. Phys. Lett.* 85 (2004) 3617–3619.
- [27] J. Luschitz, K. Lakus-Wollny, A. Klein, W. Jaegermann, Growth regimes of CdTe deposited by close-spaced sublimation for application in thin film solar cells, *Thin Solid Films* 515 (2007) 5814–5818.
- [28] H.R. Moutinho, R.G. Dhere, M.M. Al-Jassim, C. Ballif, D.H. Levi, A.B. Swartzlander, M.R. Young, L.L. Kazmerski, Study of CdTe/CdS solar cells using CSSCdTe deposited at low temperature, in: Proceedings of the 28th IEEE Photovoltaic Specialists Conference, 2000, pp. 646–649.
- [29] J.D. Major, L. Bowen, R.E. Treharne, K. Durose, Assessment of Photovoltaic Junction Position in CdTe Solar Cells Using a Combined FIB-EBIC Technique, *MRS Proceedings*, 143, 2, 2012, mrs12-1432-g11-06
- [30] J.J. Wang, T. Ling, S.-Z. Qiao, X.-W. Du, Double open-circuit voltage of three-dimensional ZnO/CdTe solar cells by a balancing depletion layer, *ACS Appl. Mater. Interfaces* 6 (2014) 14718–14723.